Ocean Engineering 89 (2014) 230–242

Contents lists available at ScienceDirect

Ocean Engineering

journal homepage: www.elsevier.com/locate/oceaneng

Reliability-based fatigue life investigation for a medium-scale composite hydrokinetic turbine blade

H. Li [a], Z. Hu [a], K. Chandrashekhara [a,*], X. Du [a], R. Mishra [b]

[a] Department of Mechanical and Aerospace Engineering, Missouri University of Science and Technology, Rolla, MO 65409, USA
[b] Department of Materials Science and Engineering, University of North Texas, Denton, TX 76203, USA

ARTICLE INFO

Article history:
Received 16 October 2013
Accepted 8 August 2014

Keywords:
Fatigue
Reliability
Blade element momentum
Finite element method
Hydrokinetic
Composite blade

ABSTRACT

As the most important, expensive component of a hydrokinetic turbine system, the composite turbine blade must achieve a long operating life (10–20 years). The investigation of fatigue life for the composite turbine blade is essential when designing a cost-effective hydrokinetic composite turbine system. A reliability-based fatigue life analysis methodology was developed for a medium-scale, horizontal axis, hydrokinetic turbine blade. Finite element method, coupled with the blade element momentum theory, was used to find the stress response on the turbine blade. The fatigue behavior of the blade was studied in stress-critical zones. A metamodel was constructed for the stress response according to simulations at specified design points. Accounting for uncertainties in material properties and the material *S–N* curve, the reliability analysis method was employed to estimate the fatigue life distribution of the hydrokinetic turbine blade. The effect of river velocity models on the fatigue life of turbine blades was also studied. The fatigue life of the composite blade was sensitive to composite material properties. Transverse strain E_{22} is particularly dominant which is related to the matrix cracking as the fatigue failure mode. The statistical distribution of *S–N* data implies a significant dependence of fatigue life on composite *S–N* data.

1. Introduction

Hydrokinetic turbines contribute to zero-head hydropower. The turbines use hydrokinetic power from flowing water to generate power. In many ways, hydrokinetic turbines resemble wind turbines. The most notable difference is in density; the density of water is approximately 850 times greater than the density of air. Thus, more energy is expected from a hydrokinetic turbine. Due to the vast resources of hydrokinetic/tidal energy on earth the research into hydrokinetic/tidal turbine systems, as an alternative renewable energy, has been booming in recent years (Khan et al., 2009; Schwartz, 2006).

The blade is the key component in a hydrokinetic turbine system; it determines the performance of the turbine system. A hydrodynamic profile design of the turbine blade is required to extract the maximum energy from water flow. Environmental conditions must be considered when designing the blade. Varying hydrokinetic loadings, water/mud corrosion and impact from floaters and fish schools each has a significant effect on the blade's operating life. From a structural point of view: (1) the hydrokinetic turbine blade is long and flexible; (2) there are possibilities of vibrations in the resonant mode; (3) the randomness of water velocity causes randomness of load spectra; and (4) low maintenance is expected during operating under water with different conditions (Shokrieh and Rafiee, 2006). Load identification, geometry/structural design, static failure, and fatigue failure all need to be addressed to create a successful blade design.

Typical fatigue loads on hydrokinetic turbine blades include stochastic hydrodynamic loadings from water streams, weight and buoyancy of the composite blade, and induced centrifugal and coriolis force (Nijssen, 2006). The stochastic hydrokinetic loadings include the flapwise loads and the edgewise loads. The flapwise loads originate primarily from the water load. This load acts perpendicular to the rotor plane. The edgewise loads originate primarily from the blade weight, buoyancy forces from water volumes occupied by the blade body, and also the torque loads that drive the rotor. The loading direction for edgewise loads changes twice during a revolution.

As regards materials, attractive characteristics of composites like light weight, high strength/stiffness, design flexibility and corrosion resistance (as compared to metallic materials) make composite materials an advantageous option for river applications. Based on these characteristics of composites, manufacturing using composites is capable of achieving a structural design with a complicated geometric layout and adequate load-carrying capacity while achieving significant weight reduction.

* Corresponding author. Tel.: +1 573 341 4587.
E-mail address: chandra@mst.edu (K. Chandrashekhara).

http://dx.doi.org/10.1016/j.oceaneng.2014.08.006
0029-8018/

The manufacturing process for composite structures is quite complex. As a result, various parameters can influence the fatigue behavior of composites in terms of fiber/matrix type, reinforcement structure, laminate stacking sequence, environmental conditions (both temperature and moisture), and loading conditions (stress ratio, frequency) (Degrieck and Paepegem, 2001). The damage accumulation of composites from these factors may either independently or interactively affect fatigue life. Over the last several decades, various fatigue damage models of fiber reinforced composite materials have been developed. These models can be mainly categorized into three sections: (1) *S–N* curves/Goodman diagrams incorporating fatigue failure criterion with no degradation mechanisms, (2) phenomenological models based on residual stiffness/strength, and (3) progressive damage models utilizing damage variables to characterize different damage mechanisms (e.g. matrix cracks and delamination). Detailed discussions on the development of fatigue damage models of fiber-reinforced composite materials can be found in review papers (Degrieck and Paepegem, 2001; Post et al., 2008).

The fatigue life of composites for wind turbine blade applications has been studied considerably as a result of the rapid growth in the wind industry. A Department of Energy/Montana State University (DOE/MSU) composite material fatigue database for wind blades (Mandell and Samborsky, 2010) was established under sponsorship of Sandia National Laboratories (SNL). The database includes detailed fatigue results for composite materials under constant/variable amplitude fatigue loadings. Sutherland and Mandell (2005a, 2005b) studied the effect of both mean stress and an optimized constant-life diagram on the damage of wind turbine blades. Samborsky et al. (2008) investigated the fatigue loading effect on delamination at thick ply drops in both carbon and glass fiber laminates. Comparatively, study regarding composites used for hydrokinetic/tidal applications is still much less. Some preliminary studies can be seen in Mahfuz and Akram (2011), Kennedy et al. (2011), and Li et al. (2012).

Fatigue loads on hydrokinetic turbine blades have a certain degree of statistical variability. These factors comprise material variability, variable water velocity, and scattered *S–N* data. Young et al. (2010) quantified the influence of material and operational uncertainties on the performance of self-adaptive marine rotors. A reliability based design and optimization methodology for adaptive marine structures was developed. Lange (1996) found that fatigue reliability is significantly dependent on the type of model chosen. An increasing spread in failure probabilities for a given turbine life was observed in flatter *S–N* curves. Blade-to-blade variation has been characterized very little due to the complexity of composite manufacturing processes (Nijssen, 2006). Hence, the reliability method should be introduced into the fatigue analysis of composite blades.

The study on composite blades for hydrokinetic applications is very limited and there is a lack of complete characterization of factors' effect (material, flow, and fatigue data) on the fatigue life. The purpose of this paper is to quantify the effects of material, loading uncertainties on the stress response and fatigue data on the fatigue life distribution of a medium-scale hydrokinetic composite turbine blade. The optimized composite turbine blade is intended to be deployed in Missouri River. A fully-coupled blade element momentum-finite element method (BEM-FEM) was used to compute the stress response of the turbine blade. Modeling uncertainties were conducted with the Hashin failure initiation model to correlate with the fatigue failure mode of the turbine blade. The fatigue model was based on both MSU/DOE experimental *S–N* data and the residual strength approach to cumulative damage. The probability of fatigue failure was evaluated. The effects of the river flow velocity model were investigated on the fatigue probability distribution of the turbine blade.

2. Structural design of the composite blade

2.1. Hydrodynamic profile

The composite blade was designed for three-blade, horizontal axis, hydrokinetic turbine systems. It has a length of 1 m, and varying cross sections with an 8° twist angle. The circular root section was designed for easy mounting on the hub. The blade consisted of eight blade stations, as shown in Fig. 1. The blade profile was based on hydrofoil Eppler 395. The hydrofoil provides a high ratio of C_l/C_d. Detailed identification of both the hydrodynamic profile and the corresponding hydrodynamic loadings on the blade surface, with varying tip speed ratio (TSR), is illustrated in Section 3.

2.2. Facesheet and core materials

Hydrokinetic turbine systems operating under water experience highly repetitive hydrodynamic loadings. Also, bio-fouling and corrosion issues need to be addressed properly. The hydrokinetic turbine blade facesheet made of composite materials with a high modulus and strength provides excellent static failure resistance. Corrosion issues can also be effectively prevented with the use of composite materials (Anyi and Kirke, 2010). Widely used carbon fibers normally cost 10–20 times as much as glass fibers. Carbon fibers do, however, provide a much higher modulus and weight reduction. An E-glass/epoxy material was selected as a compromise between price and performance. Initial work on the blade design was conducted based on both trial and error and numerical optimization methods (Li and Chandrashekhara, 2012). In the current study, E-glass/epoxy laminates with $[0_2/90_2/0_2/90_2]$ ply orientations were used to form the facesheet of the hydrokinetic turbine blade. Each ply thickness was 0.356 mm.

Various blade core configurations were evaluated to obtain an optimal blade internal structural layout (Berry, 2007): hollow, solid foam, composite shear web, and both foam and shear web, as illustrated in Fig. 2. Blades with a facesheet tend to provide only the lightest solution when operating under water. Water impermeability is prevented as water is prone to intrude the cavity of the blade. The water intrusion causes extra dynamic loadings when the blade rotates and significantly reduces the fatigue life of the blade. The core material selected requires high buckling resistance, water impermeability, and high strength to weight ratios. Divinycell HCP 100 was selected to provide excellent hydraulic compressive properties, a closed cell structure with very low buoyancy loss, and water absorption under long-term loading conditions. Moreover, HCP 100 offers excellent ductile characteristics; it is suitable for hydrokinetic turbine blades which experience either impact or slamming loads from floaters and schools of fish. Given the water impermeability of the turbine blade, the weight of the turbine blade tends to be offset by neutral buoyancy. The buoyancy from the core material is beneficial for a fatigue load reduction of the rotor and a higher power extraction from water. However, it seems insufficient with only solid foam to withstand shear loading. Thus, the concept of a shear web was introduced. Therefore solid foam, combined with a shear web, was adopted for the blade core design to provide water impermeability and maintain a shear loading capacity.

2.3. Failure mode of the composite blade

An appropriate damage initiation model must be chosen to evaluate the failure mode of the composite blade. Unlike maximum stress/strain, the Tsai–Hill and Tsai–Wu criterion, Hashin damage considers four different failure modes: fiber tension, fiber compression, matrix tension, and matrix compression. Failure in the ply thickness direction is ignored. Hashin damage predicts the dominating factor that influences the cracking/failure of the composite blade. Predictions from Hashin damage were used in

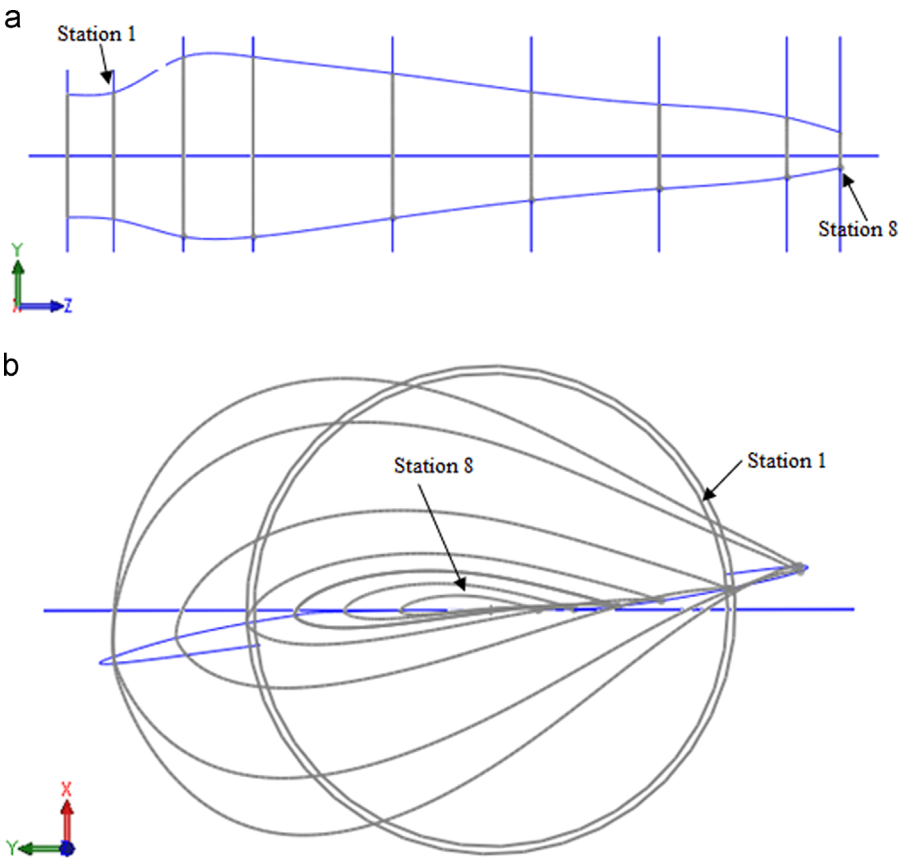

Fig. 1. Hydrodynamic profile of the hydrokinetic composite blade. (a) Longitudinal view of the blade stations and (b) cross-sectional view of the blade stations.

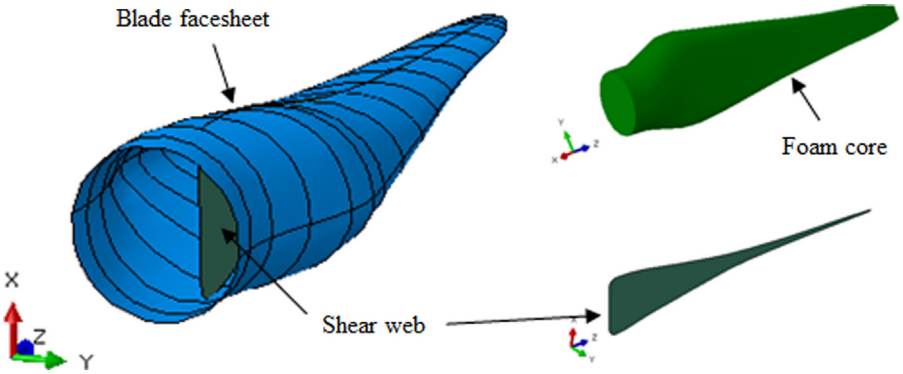

Fig. 2. Configuration of the composite blade structure.

this study to provide both the critical material points and the corresponding failure modes necessary for fatigue failure evaluation. The initiation criteria (Hashin, 1980) used was as follows:

- fiber tension ($\hat{\sigma}_{11} \geq 0$) $F_f^t = \left(\frac{\hat{\sigma}_{11}}{X^T}\right)^2 + \alpha\left(\frac{\hat{\tau}_{12}}{S^T}\right)^2$
- fiber compression ($\hat{\sigma}_{11} < 0$) $F_f^c = \left(\frac{\hat{\sigma}_{11}}{X^C}\right)^2$
- matrix tension ($\hat{\sigma}_{22} \geq 0$) $F_m^t = \left(\frac{\hat{\sigma}_{22}}{Y^T}\right)^2 + \left(\frac{\hat{\tau}_{12}}{S^L}\right)^2$
- matrix compression ($\hat{\sigma}_{22} < 0$)

$$F_m^c = \left(\frac{\hat{\sigma}_{22}}{2S^T}\right)^2 + \left[\left(\frac{Y^C}{2S^T}\right)^2 - 1\right]\frac{\hat{\sigma}_{22}}{Y^C} + \left(\frac{\hat{\tau}_{12}}{S^L}\right)^2 \quad (1)$$

where F represents the typical failure initiation prediction (a value greater than 1 indicates failure); superscripts t/T and c/C represent tension and compression, respectively, subscripts f and m represent fiber and matrix, respectively; X, Y and S represent the longitudinal, transverse and shear strength, respectively; S^L and S^T represent the longitudinal and transverse shear strength, respectively; α is the coefficient that determines the contribution of the shear stress to the fiber tensile initiation criterion; $\hat{\sigma}_{11}, \hat{\sigma}_{22}$, and $\hat{\tau}_{12}$ are components of the effective stress tensor.

Stress from each ply through the blade thickness was calculated to identify structural failure of the composite blade under applied hydrodynamic loadings. The Hashin failure criterion was then applied based on current stress conditions. The first ply failure (FPF) was regarded as the structural failure initiation of the hydrokinetic turbine blade (Zhang and Yang, 2009). The composite blade of the current design should not experience stress higher than that of FPF. Detailed implementation of the methodology in the finite element model of composite blades is illustrated in detail in Section 3. Table 1 lists the structural performance of the

Table 1
Static stress evaluation for different blade configurations.

Blade configuration	Hollow	Foam	Shear web
Weight (kg)	2.07	5.62	2.66
Buoyancy (N)	–	86.9	–
Deflection under hydrodynamic loadings (m)	0.025	0.022	0.021
Maximum Hashin failure index	0.4638	0.2865	0.4405
Location	Root section	Stations 5, 6	Root section

composite blades under specified hydrodynamic loadings. Three blade configurations were evaluated at water velocity 2.47 m/s. Fig. 3 illustrates the critical stress spots within the turbine blades. The maximum Hashin failure index the blade experienced was reduced by 38.2% when foam was present; the critical stress spot was transferred to stations 5 and 6. The complete design of the blade (with foam) greatly relieved stress at the root section, though it added more weight to the entire rotor system. This weight, however, was alleviated by the buoyancy the foam provided. Both the hollow blade and the blade with solid foam tended to have high stress values only in the region between stations 4 and 6. The existence of a shear web significantly reduced the stress level at the outer bound of the blade; it effectively prevents buckling/breakage of the blade at outer bound.

3. BEM–FEM coupled method

The BEM–FEM coupled method determines the stress response of the composite turbine blade at any given hydrokinetic loading condition. Computational fluid dynamics (CFD) analysis tends to give more detailed and accurate fluid effect on the turbine blade. However, the BEM–FEM coupled method proposed in this paper is capable of yielding faster and more efficient solutions for any specified blade geometry/structure configurations. Parametric studies of reliability-based fatigue analysis could be achieved in significantly less time. It is especially time-saving under the circumstance that significant sampling points are required to construct the stress response of the blade. Fig. 4 illustrates a flowchart of the BEM–FEM coupled method developed. The method uses Xfoil to obtain the hydrodynamic coefficients of hydrofoils at different stations. With the input from real time flow velocity and the blade geometric configuration, the real time hydrodynamic forces were calculated using the BEM method in MATLAB. The forces were the input to the finite element model using ABAQUS. Based on the existing blade structural lay-up, structural response of the blade was obtained. The stress analysis results of ABAQUS were then transferred back to MATLAB for post-processing. During the next step of the analysis, water velocity model will be called again for an updated flow velocity. Every data point obtained from the analysis as the input to the fatigue reliability computational block was processed in MATLAB as well.

3.1. Hydrodynamic performance of hydrofoils

The baseline blade construction was based on hydrofoil Eppler 395, as shown in Fig. 5. Fully hydrodynamic performance of Eppler 395, namely lift/drag coefficients, needs to be characterized at specified angle of attacks/Reynolds numbers. The smooth geometric transition between blade root section and tip indicates hydrodynamic characteristic variation at different blade cross sections as well. Xfoil (Drela, 2006), which is widely accepted as an effective tool for low Reynolds number airfoil design, was used to address this issue. Xfoil combines second-order panel method and fully-coupled viscous/inviscid interaction. The software is

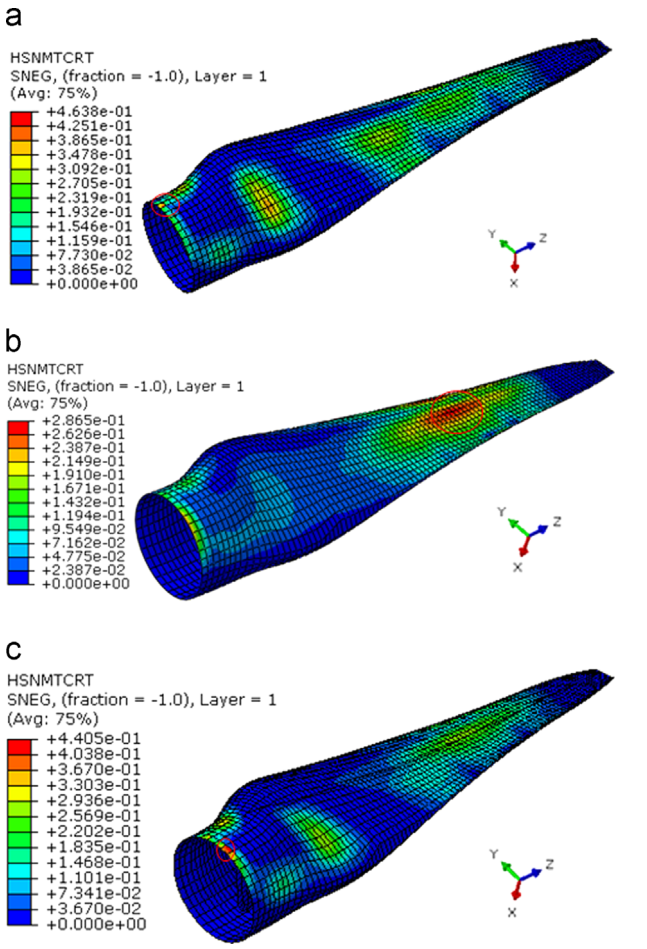

Fig. 3. Critical position of stress concentration for different blade configurations. (a) Hollow blade (at the root), (b) blade with foam (at stations 5-6) and (c) blade wtith a shear web (at the root).

capable of simulating small to medium flow separation and yielding acceptable results for large flow separation. Coefficients of drag/lift both at the Reynolds number of turbine operation and a low range of angle of attack [0°,15°] were calculated to obtain accurate results.

Inputting BEM, however, requires a complete hydrofoil dataset at each cross-section over a [−180°,180°] range angle of attack. The hydrofoil table from Xfoil was extended to large angles of attack using the Viterna method (Viterna and Janetzke, 1982):

$$C_{D_{max}} = 1.11 + 0.018AR$$
$$C_D = C_{D_{max}} \sin^2\alpha + B_2 \cos\alpha$$
$$C_L = \frac{C_{D_{max}}}{2} \sin 2\alpha + A_2 \frac{\cos^2\alpha}{\sin\alpha} \quad (2)$$

where $B_2 = C_{D_s} - C_{D_{max}} \sin^2\alpha_s / \cos\alpha_s$, $A_2 = (C_{D_s} - C_{D_{max}} \sin\alpha_s \cos\alpha_s) \sin\alpha_s / \cos^2\alpha_s$, s denotes the value at the stall angle, and AR is the blade aspect ratio. A smooth, geometric transition exists between the root section and the blade tip. Thus, unknown hydrodynamic characteristics from transitional cross-sections (blend hydrofoil) are obtained by weighting. Figs. 6 and 7 illustrate the typical lift coefficient and drag coefficient, respectively, including all 8 stations in the range [−180°,180°] after interpolation and weighting.

3.2. Hydrokinetic loadings on the turbine blade

The BEM theory is an extension of the actuator disk theory. This theory combines the conservation of momentum theory with the

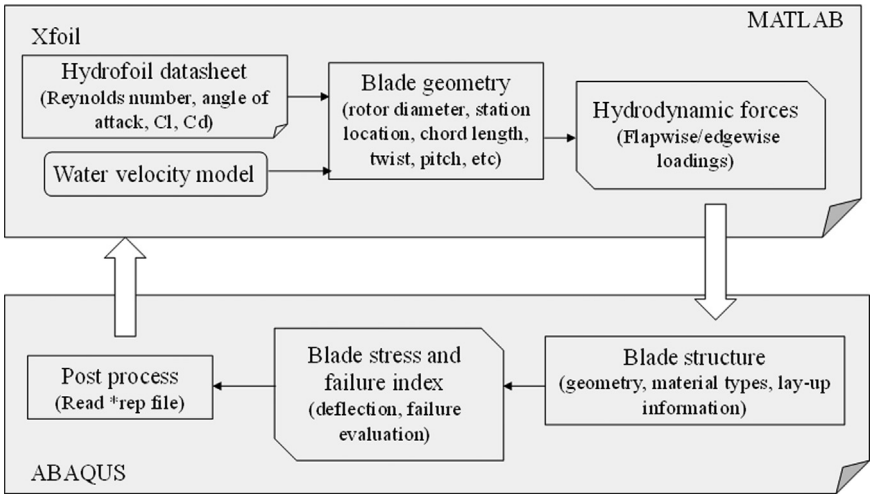

Fig. 4. Flowchart of the BEM–FEM coupled model.

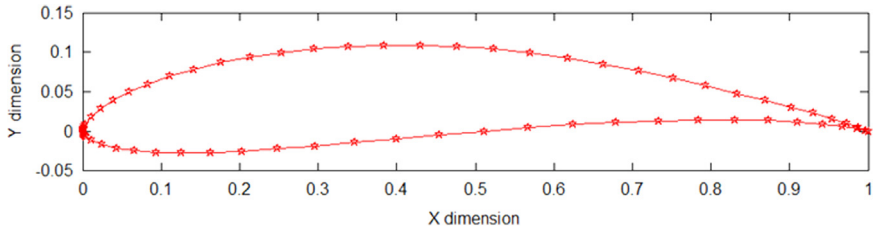

Fig. 5. Geometry profile of Eppler 395.

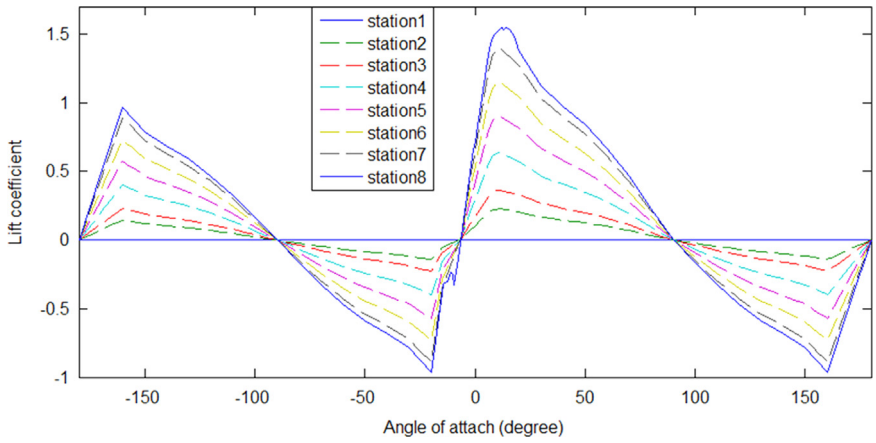

Fig. 6. Lift coefficient with angle of attack at each station.

blade element theory (Buckland et al., 2010). No-radial-dependency is assumed. As stated BEM, compared to CFD analysis, is capable of giving time-efficient and reliable solutions at any given blade geometry, pitch angle, angular velocity and river velocity. Fatigue analysis would also be an intensive calculation process due to the variability of the water velocity model and uncertainties within the materials. BEM was adopted in this study to calculate the loads on the blade surface. Prandtl tip loss, Glauert correction and hub loss were incorporated in BEM to improve solution accuracy (Sale et al., 2009).

Fig. 8 illustrates the induced velocity field around a hydrofoil. The induced velocity in the axial direction is specified with the axial induction factor a as aV_o, where V_o is the undisturbed water velocity. The induced tangential velocity in the rotor wake is specified with the tangential induction factor a' as $a'\omega r$. Variable ω represents the angular velocity of the rotor, and r is the radial distance from the rotational axis. Variable ϕ is the flow angle, θ is the sectional pitch angle, and α is the local angle of attack. Variable α is used to interpolate from hydrofoil table to get the corresponding C_l and C_d.

The Prandtl tip loss model corrects the assumption of an infinite number of blades. The model estimates the influence of vortices, which are shed from the blade tips, on the induced velocity field in the rotor plane. Equations accounting for the blade tip loss, hub loss, and their combined effect are given by

$$F_{tip} = \frac{2}{\pi}\cos^{-1}\left[e^{-\frac{B}{2}\frac{(L-r)}{r\sin\phi}}\right]$$

$$F_{hub} = \frac{2}{\pi}\cos^{-1}\left[e^{-\frac{B}{2}\frac{(r-R_{hub})}{R_{hub}\sin\phi}}\right]$$

$$F = F_{tip}F_{hub} \tag{3}$$

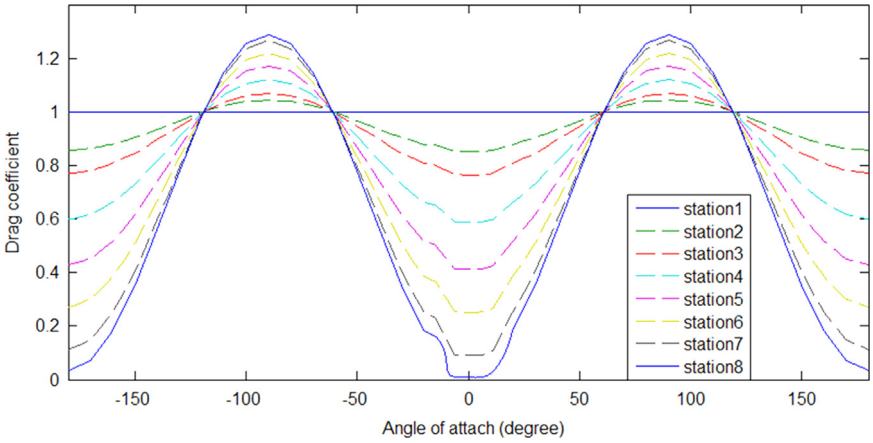

Fig. 7. Drag coefficient with angle of attack at each station.

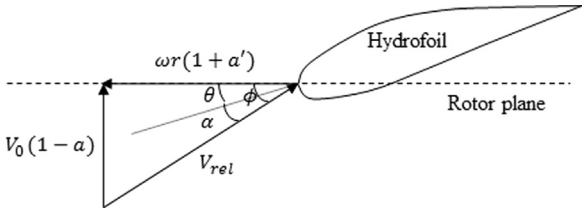

Fig. 8. Velocity vectors around a certain blade station.

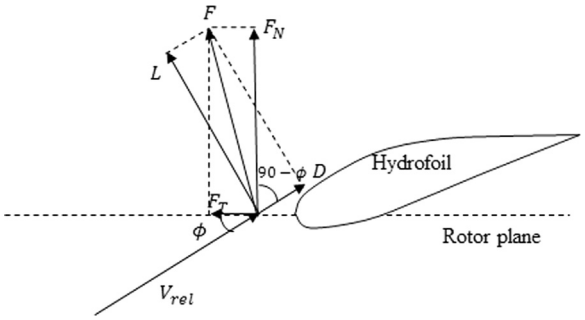

Fig. 9. Load integration on a typical hydrofoil.

where L is the blade length, $R_{hub}$is the radius of the hub, and B is the number of blades.

With a known section angle of attack, both the lift coefficient (C_l) and the drag coefficient (C_d) were extracted from the hydrofoil table at every iteration.

BEM is typically an iterative process. The thrust coefficient is an indicator to update both a and a' at each iteration with

$$C_T = \frac{\sigma(1-a)^2(C_l \cos\phi + C_d \sin\phi)}{\sin^2\phi} \tag{4}$$

where σ is the blade element solidity. Both a and a' are then updated for the next iteration, when $C_T \le 0.96F$:

$$a = \left[1 + \frac{4F\sin^2\phi}{\sigma(C_l \cos\phi + C_d \sin\phi)}\right]^{-1} \tag{5}$$

If $C_T > 0.96F$, the blade element is highly loaded and operates in a turbulent wake state. A modification to the Glauert empirical relation was applied (Buhl, 2004). Variable a is instead updated with

$$a = \frac{18F - 20 - 3\sqrt{C_T(50-36F)+12F(3F-4)}}{36F-50} \tag{6}$$

Meanwhile, a' is updated with

$$a' = \left[\frac{4F\sin\phi\cos\phi}{\sigma(C_l \sin\phi - C_d\cos\phi)} - 1\right]^{-1} \tag{7}$$

Once the iterative process converges, and the induction factors have been obtained at every blade element, the relative water velocity can be obtained with $V_{rel} = \omega r(1+a')/\cos(\phi)$. As the lift and drag coefficients (C_l and C_d) were extrapolated from the hydrofoil table the lift (L) and drag (D), per station length, can be computed with

$$L = \frac{1}{2}\rho V_{rel}^2 c C_l$$
$$D = \frac{1}{2}\rho V_{rel}^2 c C_d \tag{8}$$

Both the force normal and tangential to the rotor plane, as shown in Fig. 9, can then be obtained with

$$F_N = L\cos\phi + D\sin\phi$$
$$F_T = L\sin\phi - D\cos\phi \tag{9}$$

These loads serve as the input to the finite element model.

The hydrodynamic loadings obtained from MATLAB simulation were validated with Bladed Tidal (Garrad Hassan, 2012) for the demo blade provided by the software. The validation ensures fidelity of the hydrodynamic load input to the finite element model of the blade. The demo blade was intended for a three-blade tidal turbine system. It was 10.5 m long with an 8.5° twist. It operated at a tidal velocity of 3 m/s and a fixed pitch of 0°. The tip speed ratio (TSR) was equal to 3 (i.e., rotational velocity was 7.54 rpm). Numerical analysis solutions were obtained from both the in-house code and Blade Tidal. A verification of the results in terms of axial/tangential induction factors, lift/drag coefficient, and normal/tangential forces along the blade was conducted. Fig. 10 demonstrates comparison of normal (out-of-plane) and tangential (in-plane) forces for the specific case between two codes.

3.3. Finite element model of the turbine blade

Finite element method was used to identify the turbine blade's critical stress spots. It was also used to evaluate the blade's structural failure. The commercial software package ABAQUS 6.10 (Dassault Systèmes, 2010) was used for the stress analysis of the composite blade. Table 2 lists the material properties of the E-glass/epoxy lamina used in the simulation. The BEM code's output was in-plane/out-of-plane hydrokinetic loadings, per unit length, on the blade's surface. These loadings were integrated over adjacent blade stations. Each station span (8 in total) was applied

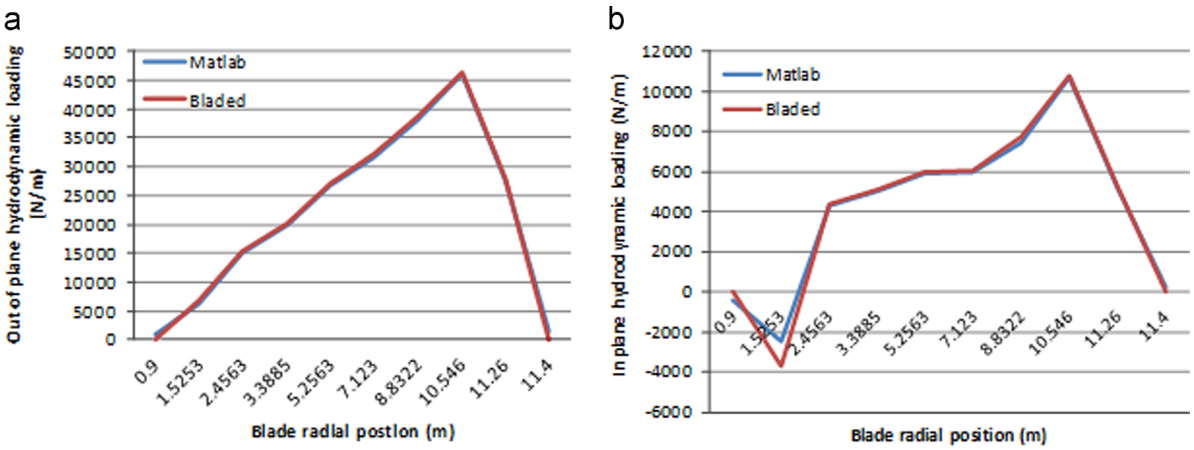

Fig. 10. Comparison of hydrodynamic loadings on the composite blade between the in-house MATLAB code and Blade Tidal. (a) Out-of-plane and (b) in-plane.

Table 2
Material properties of E-glass/epoxy lamina (Soden et al., 1998).

Property	Value
Young's modulus (GPa)	$E_1=45.6$, $E_2=E_3=16.2$
Poisson's ratio	$\nu_{12}=\nu_{13}=0.278$, $\nu_{23}=0.4$
Shear modulus (GPa)	$G_{12}=G_{13}=5.83$, $G_{23}=5.786$
Density (kg/m^3)	$\rho=2000$
Longitudinal tensile strength (MPa)	$X^T=1280$
Longitudinal compressive strength (MPa)	$X^C=800$
Transverse tensile strength (MPa)	$Y^T=40$
Transverse compressive strength (MPa)	$Y^C=145$
In-plane shear strength (MPa)	$S^T=S^L=73$

with concentrated hydrodynamic forces on the blade surface using the multi-point constraint (MPC) technique. Concentrated loads were applied on reference nodes sets along the pitch axis of the turbine blade. Structural distributing coupling was adopted to interconnect degrees of freedom between the control point and a certain blade station surface. The structural coupling method couples the translation and rotation of the reference node to the translation and the rotation motion of the coupling nodes, respectively. This method is well-suited for bending problems of composite blade; the coupling constraint covers small sections of nodes, and the reference node is very close to the constrained surface.

The composite blade was treated as an encastre beam with all degrees of freedom fixed at the root section. Loadings, including the weight of the composite blade $\{F_w\}$, the buoyancy force $\{F_b\}$ due to water, the induced centrifugal force $\{F_{ce}\}$, and the coriolis force $\{F_{co}\}$, were each considered when fully characterizing the turbine blade's loading condition during the operation (Young et al., 2010). The structural analysis of the rotating blade-fixed coordinate system was formulated as

$$[K]\{u\}=\{F_h\}+\{F_w\}+\{F_b\}+\{F_{ce}\}+\{F_{co}\} \tag{10}$$

where $\{u\}$ is the structural nodal displacement vector, $[K]$ is the stiffness matrix and $\{F_h\}$ is the hydrodynamic force. Fig. 11 depicts the finite element model of the composite blade. Each lay-up was modeled individually using S4R shell elements. All the forces were applied through ABAQUS load module. $\{F_h\}$ is the output from the BEM model. $\{F_w\}$, $\{F_b\}$, $\{F_{ce}\}$ and $\{F_{co}\}$ were applied in forms of periodic gravity, body force, rotational body force, and Coriolis force, respectively. The low-cycle calculation of the rotating composite blade was conducted in ABAQUS. Fig. 12 illustrates the simultaneous stress variation with time of the stress concentration spot, at the root section of the blade, under five normalized

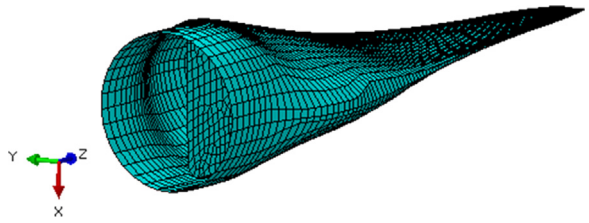

Fig. 11. Finite element model of the composite blade.

loading cycles. The stress was extracted from the surface layer (0°) of the composite blade in transverse direction.

4. Fatigue life of the composite blade

4.1. Water velocity model

The river flow velocity, which governs the fatigue life of the turbine blade, is a stochastic process. River velocity varies at different time instants due to natural variability. The design of hydrokinetic turbine systems is a relatively new research topic. Thus, no closed form is available to describe the distribution of river flow velocity. There are some researchers who have devoted efforts in the modeling of statistical distribution of river flow velocity (Beersma and Buishand, 2004; Hu and Du, 2012). However, in this paper, three common distributions were used to describe the river velocity since not enough data is available to determine the optimal for the Missouri River. The three distributions used include the normal, lognormal, and Weibull distributions. At the beginning, samples were generated for the river flow velocity for the fatigue life analysis of the composite hydrokinetic turbine blade.

The Expansion Optimal Linear Estimation method (EOLE) (Sudret, 2008) was used to generate samples for the stochastic process of river flow velocity over a time interval $[0,\ t_s]$. The time interval $[0,\ t_s]$ was divided into s time points: $(t_i)_{i=1,\ 2,\cdots,s}=(t_0,\ t_1, t_2, \ldots, t_s)$. After the discretization, the non-Gaussian distribution of river velocity $V(t)$ was transformed into a function of a standard Gaussian stochastic process, as below:

$$V(t)=F_V(U(t)) \tag{11}$$

Based on the transformation and discretization, the correlated stochastic samples of $U(t)$ was then generated using the following

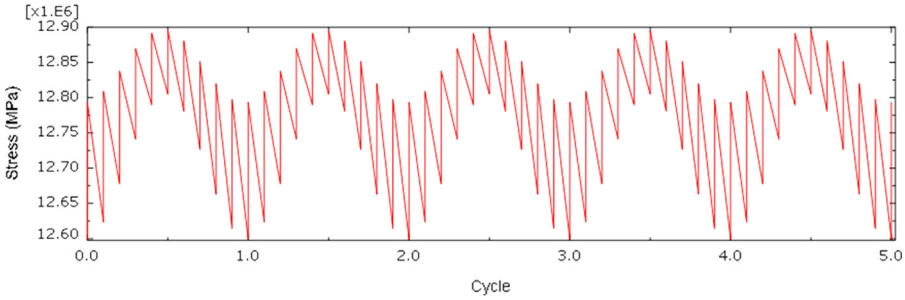

Fig. 12. Stress variation with time (stress concentration spot, root) of the optimal composite blade under cyclic loadings.

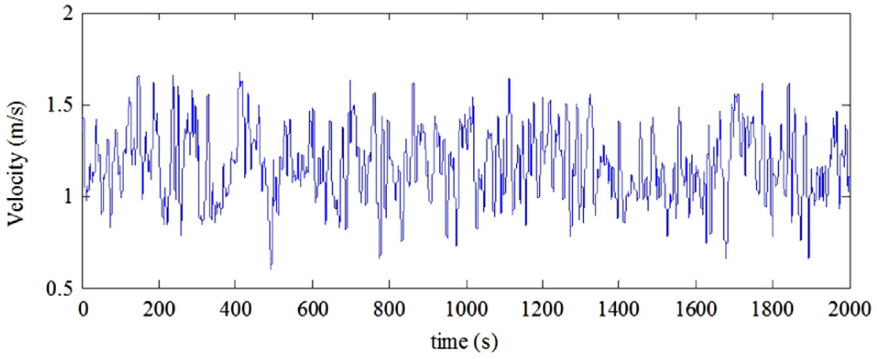

Fig. 13. A sample time history of river flow velocity (T=2000 s).

formula:

$$U(t) = \sum_{i=1}^{p} \frac{U_i}{\sqrt{\eta_i}} \varphi_i^T \rho_U(t,\ t_i) \tag{12}$$

where U_i $(i = 1,\ 2, \ldots, p \le s)$ are independent, standard, normal, random variables. Variables η_i and φ_i^T are the eigenvalues and eigenvectors of the correlation matrix (Σ), respectively, given as follows:

$$\Sigma = \begin{pmatrix} \rho_U(t_1,\ t_1) & \rho_U(t_1,\ t_2) & \cdots & \rho_U(t_1,\ t_S) \\ \rho_U(t_2,\ t_1) & \rho_U(t_2,\ t_2) & \cdots & \rho_U(t_2,\ t_S) \\ \vdots & \vdots & \ddots & \vdots \\ \rho_U(t_S,\ t_1) & \rho_U(t_S,\ t_2) & \cdots & \rho_U(t_S,\ t_S) \end{pmatrix}_{s \times s} \tag{13}$$

The ELOE method is an effective approach to generating samples for stochastic processes. River velocity samples were generated for the fatigue life analysis of the composite turbine blade with Eqs. (11)–(13). Fig. 13 displays a sample water velocity versus time.

4.2. Fatigue stress cyclic counting

The transient simultaneous stress response of the turbine blade was obtained via BEM–FEM coupled method with the aid of metamodel construction (see Section 5). The random nature of the time dependent stress spectrum requires an appropriate cycle counting algorithm. The algorithm was used to reduce the variable amplitude stress cycles into a series of simple constant stress amplitude cycles or half cycles. When compared to other counting methods (e.g., level crossing and range-mean), rainflow counting is a much better method as the mean (or R value) information is retained. In the current study, the rainflow counting algorithm which follows the ASTM standard was used (ASTM, 1985). Data extracted includes stress cycles with stress amplitude, mean stress and cycle numbers. Fig. 14 illustrates both the typical mean value and the amplitude distribution of stress cycles after applying the rainflow cyclic counting algorithm under the sample river flow velocity. Most of the cycles fall into the stress region with low mean and amplitude.

4.3. Constant-life diagram

S–N data is required to estimate the number of cycles to failure, at any specified stress amplitude, of the hydrokinetic turbine blade. The fatigue behavior of the composite blade material is, typically, fully presented as a constant-life diagram (CLD). S–N data are plotted as a function of mean stress and amplitude along lines of R values in the CLD. In the current numerical study, the normalized S–N curve of cross-ply E-glass/epoxy laminates used (R=0.1) was derived from the MSU/DOE composite fatigue database (Mandell and Samborsky, 2010):

$$\sigma_{max}/\sigma_o = 1.0 - 0.1 \log\ N \tag{14}$$

The calculated stress cycle ratio from individual stress cycle indicates very high mean stresses. Thus, a linear Goodman equation was used to correct the mean stress effect (Nijssen, 2006):

$$\frac{\sigma_a}{\sigma_{N_f}} + \frac{\sigma_m}{\sigma_0} = 1 \tag{15}$$

where σ_{N_f} is the stress amplitude for finite fatigue life N_f under fully reversed ($R = -1$) loading conditions and σ_a is the alternating stress amplitude with respect to the mean stress σ_m. R is defined by

$$R = \frac{\sigma_{min}}{\sigma_{max}} = \frac{\sigma_m - \sigma_a}{\sigma_m + \sigma_a} \tag{16}$$

where σ_{min} and σ_{max} are the minimum and maximum stress of a typical stress cycle, respectively. A full CLD was constructed based on the above calculation (Fig. 15). Less stress cycles to failure were expected for stress with either high mean or high alternative stress.

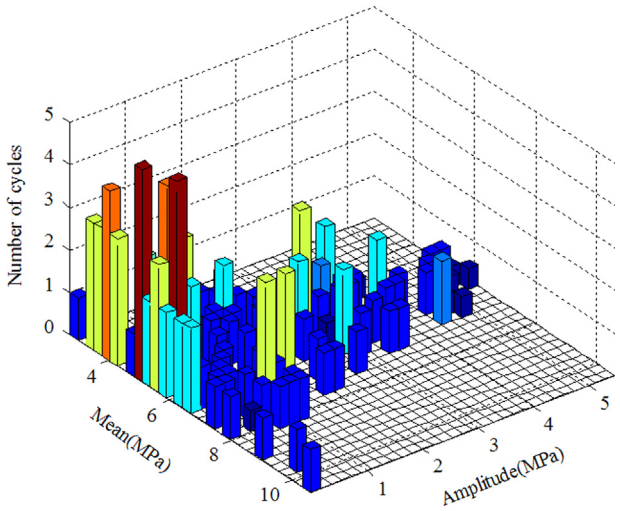

Fig. 14. Histogram of both stress amplitude and mean stress distribution in terms of cycles.

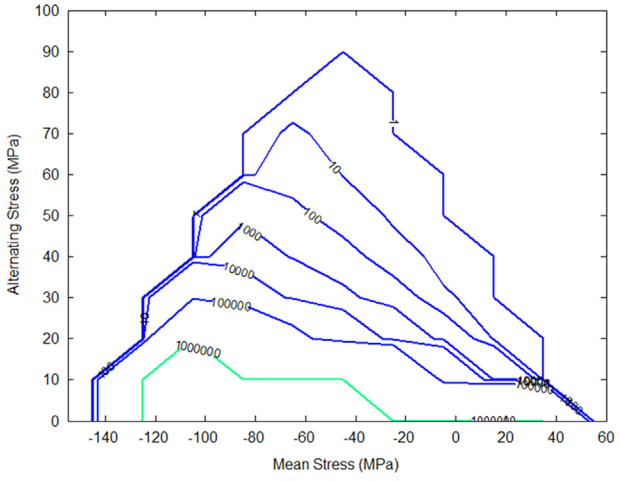

Fig. 15. Mean CLD for composite material, E-glass/epoxy [0°/90°].

4.4. Damage accumulation model

A nonlinear residual strength model (Sutherland and Mandell, 2005a, 2005b) was adopted in this study to calculate damage accumulation that leads to blade fatigue failure. The nonlinear residual strength model has the form

$$(\sigma_R)_i = \sigma_0 - (\sigma_0 - \sigma_i)\left(\frac{n_i}{N_{f_i}(\sigma_{m_i}, \sigma_{a_{ij}})}\right)^{v} \tag{17}$$

where n_i is the number of applied cycles, N_{f_i} is the number of cycles to failure at a specified stress state $(\sigma_{m_i}, \sigma_{a_i})$, $(\sigma_R)_i$ is the residual strength after step i, σ_i is the peak stress amplitude of the hydrokinetic loading at step i, σ_0 is the static strength, and v is the nonlinear degradation parameter. Failure occurs when the applied hydrokinetic loadings cannot be withstood by the residual strength of the composite blade.

5. Reliability-based fatigue life distribution

Uncertainties in the process of the fatigue life investigation were analyzed in this section. A metamodel was then constructed for the stress response of turbine blades. The fatigue life distribution, sensitivities of random variables, and effect of rive velocity model on fatigue life were then studied using the first order reliability method.

5.1. Uncertainties involved in fatigue life estimation

Uncertainties that may affect the design fatigue life of turbine blades can be divided into two categories: (1) the uncertainties in laminate properties of the composite material and (2) the uncertainties in parameters of *S–N* curve.

5.1.1. Uncertainties in laminate properties

Important parameters that influence the fatigue performance of the composite blade could be attributed to a probability of both fiber misalignment and a statistic variation of fiber/resin stiffness. Hence, six variables for material stiffness and four variables for ply-orientation were assigned with probability distributions. These variables include the elastic modulus E_{11}, $E_{22}(E_{33})$ and the shear modulus $G_{12}(G_{13})$, G_{23}. As mentioned in Section 2, the hydrokinetic turbine blade was made of E-glass/epoxy laminates with $[0^\circ_2/90^\circ_2/0^\circ_2/90^\circ_2]$ configurations. Hence, variation was also assigned to each of the ply orientations (0°_2 and 90°_2). Normally distributed and a 2% coefficient of variation (ratio of the standard deviation to the mean of a random variable) were assumed to the stiffness (Young et al., 2010). A 2° variation of ply orientation to the composite material was also assumed (Table 3).

5.1.2. Scatter in S–N data

Variation in both static strength and fatigue life is unavoidable; composite coupons tested under fatigue loadings would not be in the exactly same condition. Typically, the values of static strength scatter in glass/epoxy composites are within 10% of the mean value. The static scatter is inherently attributed to the material production (Nijssen, 2006). The scatter in fatigue strength can be related to scatter in static strength. In the current study, static data was included in *S–N* data. This data assumed that static data indicates failure in the first load cycle of material specimens. Therefore, the fatigue behavior of the chosen material can be described by static strength and a slope parameter. Conservative variations in static strength (2%) and the slope of *S–N* curve were assumed to characterize the scatter in fatigue data to avoid uncertainty overlapping with laminate properties (Fig. 16).

5.2. Construction of the metamodel

There are many kinds of metamodel techniques available, such as the response surface method, the Kriging model method (Jones et al., 1998), support vector machine (Burges, 1998), and polynomial chaos expansion (PCE) method (Xiu and Karniadakis, 2002). To account for the uncertainties in laminate properties as well as the river flow loading, herein, the PCE method was employed to construct the metamodel of stress response. Training points of input variables were generated according to their

Table 3
Probability distributions of variables from the composite laminate.

Variable	Mean	Coefficient of variation	Distribution type
Young's modulus	$E_{11}=45.6$ GPa	0.02	Gaussian
	$E_{22}=E_{33}=16.2$ GPa	0.02	
Shear modulus	$G_{12}=G_{13}=5.83$ GPa	0.02	
	$G_{23}=5.786$ GPa	0.02	
Ply orientation (deg)	First ply=0	2	
	Second ply=90	2	
	Third ply=0	2	
	Fourth ply=90	2	

probability distributions. BEM–FEM analyses were then performed at the training points. After that, the metamodel was constructed using the PCE method and the accuracy of metamodel was verified by checking the coefficients of determination. More details about the PCE method can be found in Hosder et al. (2010). In the subsequent subsections, the detailed implementation procedure is explained.

5.2.1. Sampling of random variables

Samples of random variables were generated to construct metamodels. These samples were generated according to both the distribution of random variables and their bases for expansion. To evenly generated samples over the design space, the Hammersley sampling method was employed to generate training samples (Chen et al., 1995). The number of variables intended to be expanded required a number of 265 samplings. Typical samples with both distributed material properties and lay-up information are presented in Fig. 17.

5.2.2. Stress response

BEM–FEM coupled analysis was performed at the training points. Structural evaluation of the composite turbine blade was conducted to obtain the failure mode of the blade under varying hydrokinetic loadings (see Section 2). Matrix cracking in the transverse direction on the top layer was found to be the most dominate fatigue failure indicator. Based on these studies a stress response, with respect to the matrix crack failure mode, was developed with the polynomial chaos expansion (PCE) method. In the PCE method, the river velocity was expanded using the Legendre polynomials and the other uncertain variables which follow Gaussian distribution were expanded using the Hermite polynomials. Fig. 18 depicts the stress values of the matrix in tension (from samplings versus the metamodel prediction). Results indicate that the metamodel predicts stress response very well. The metamodel is capable of yielding stress response of the blade under specified water velocities. The stress response as a function of random variables is depicted in Fig. 19.

5.3. First-order reliability method (FORM)

The first-order reliability method (FORM) was employed to perform the reliability-based fatigue life investigation to account for uncertainties in the design process. A generalized limit-state function is in the form $G = g(\mathbf{X})$ with a vector of random variables $\mathbf{X} = [X_1, X_2, \ldots, X_n]$. The probability of failure has the form $p_f = \Pr\{G = g(\mathbf{X}) < 0\}$. The following integral needs to be solved to estimate the failure probability:

$$p_f = \Pr\{G = g(\mathbf{X}) < 0\} = \int_{g(\mathbf{X}) < 0} f_{\mathbf{X}}(\mathbf{X}) d\mathbf{X} \tag{18}$$

where $f_{\mathbf{X}}(\mathbf{X})$ represents for the joint PDF of random variables $\mathbf{X}$.

The integral in Eq. (18) is usually a high-dimensional integration. This integration is very difficult to solve directly. Ten random

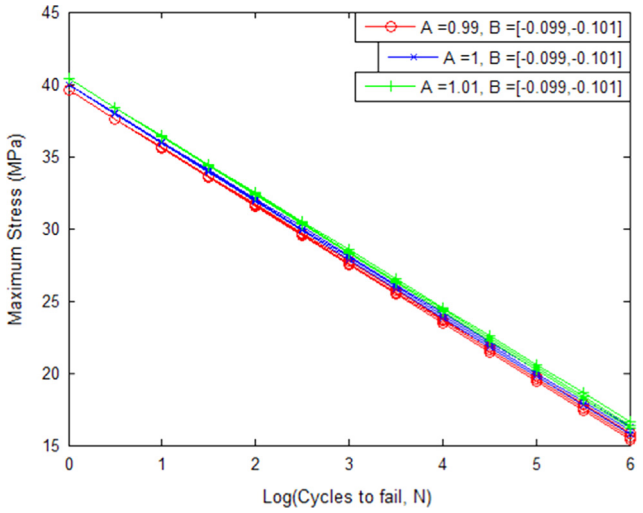

Fig. 16. Scatter of S–N data (R=0.1).

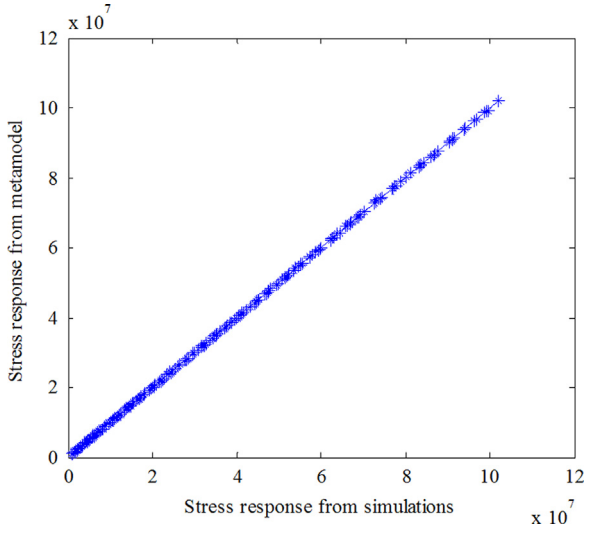

Fig. 18. Predicted stress values compared to solution from sampling points.

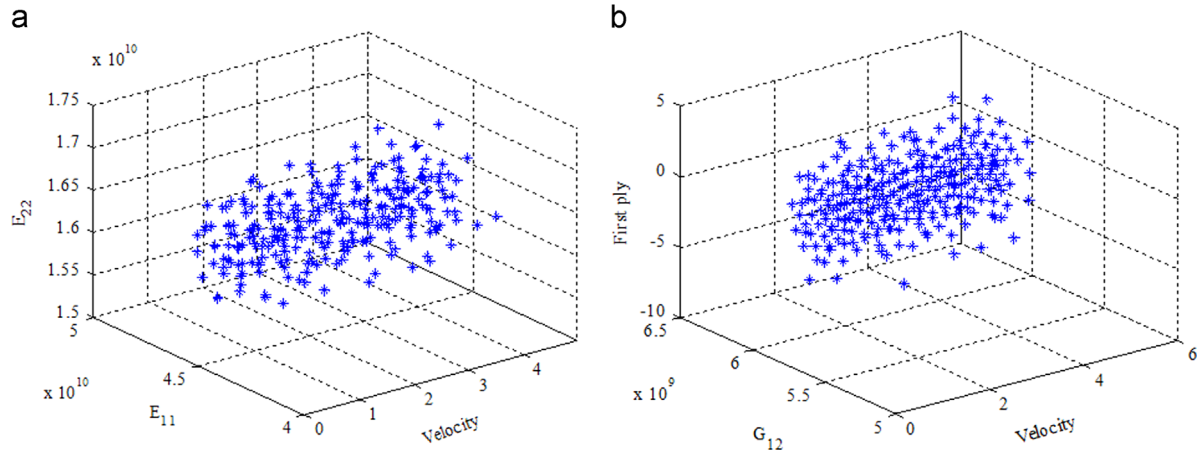

Fig. 17. Samples of random variables regarding both material properties and ply-orientation. (a) E11, Velocity and E22 and (b) G12, Velocity and First ply.

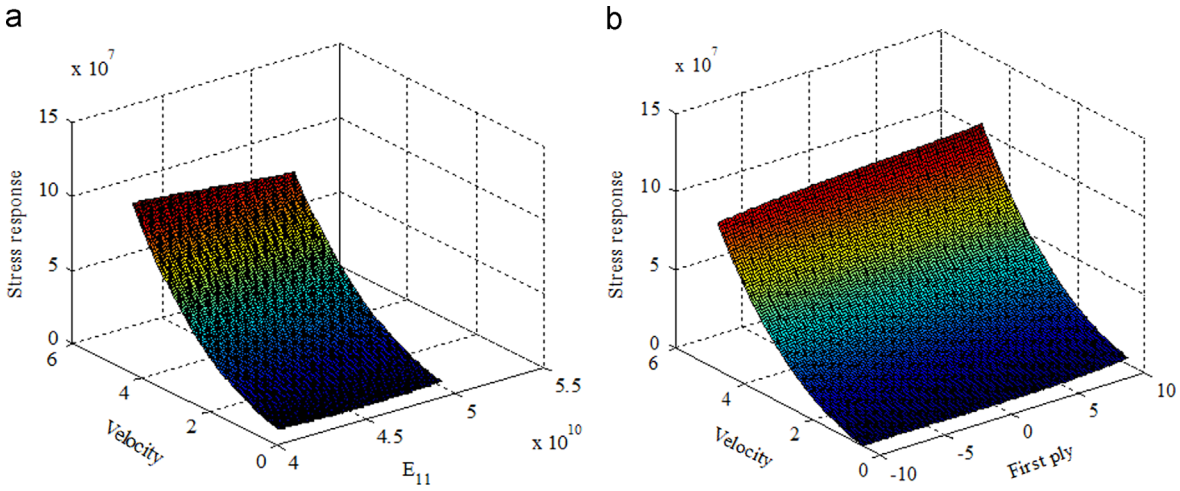

Fig. 19. Response surface of matrix tensile stress. (a) Velocity, E11 and Stress response and (b) velocity, First ply and Stress response.

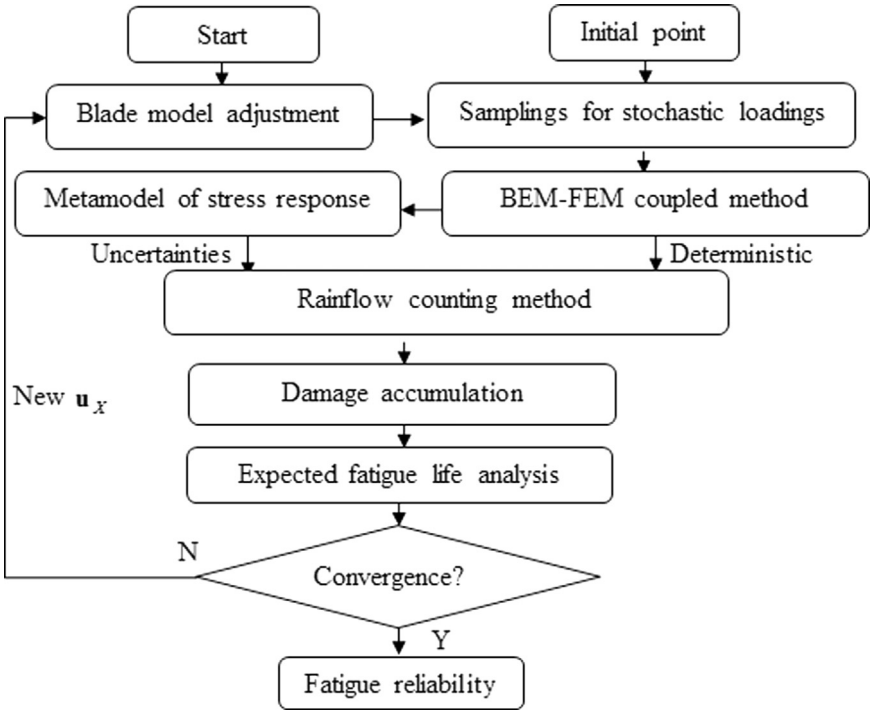

Fig. 20. Fatigue reliability analysis of hydrokinetic turbine blade.

variables were involved in the reliability-based fatigue life analysis of turbine blades. The integral was, therefore, ten-dimensional.

FORM, the most commonly used reliability analysis method, has been applied in various areas where uncertainties are presented (Hu et al., 2012). The FORM approximates the limit-state function $G=g(\mathbf{X})$ by the first order Taylor expansion method. The integral in Eq. (18) was then estimated in the standard Gaussian space by linearizing the limit-state function at the most probable point (MPP).

Random variables **X** were transformed into standard Gaussian random variables **U** before applying FORM, as follows:

$$\Phi(U_i)=F_{X_i}(X_i) \tag{19}$$

and

$$U_i=\Phi^{-1}(F_{X_i}(X_i)) \tag{20}$$

in which $\Phi(\cdot)$is the CDF of a standard Gaussian random variable, $F_{X_i}(\cdot)$is the CDF of the random variable X_i, and U_i is the standard Gaussian random variable corresponding to random variable X_i.

After the transformation, the limit-state function becomes$G=g(T(\mathbf{U}))$, where $T(\cdot)$ is the operator used to transform **U** to **X**. The MPP point, where the joint PDF $f_{\mathbf{X}}(\mathbf{X})$ has the highest probability density, was then obtained by solving the following optimization model:

$$\begin{cases} \min \ \|\mathbf{u}\| \\ \mathbf{u}=[u_1,\ u_2,\ \ldots,\ u_n] \\ x_i=F_{X_i}^{-1}(\Phi(u_i)),\ i=1,\ 2,\ \ldots,\ n \\ G=g(\mathbf{x})=0 \end{cases} \tag{21}$$

Once the MPP $\mathbf{u}^*$ is obtained, the probability of failure in Eq. (11) was approximated with (Du and Chen, 2000)

$$p_f=\Pr\{G=g(\mathbf{X})<0\}=\Phi(-\beta) \tag{22}$$

where β is the reliability index. The index is given by

$$\beta = \|\mathbf{u}^*\| \tag{23}$$

5.4. Fatigue life distribution

A detailed numerical procedure (summary of the numerical implementation above) is shown in Fig. 20. A brief description of the flowchart according to the sequence of dataflow is illustrated, as follows:

i. blade hydrodynamic/structural design—design the blade shape and structural lay-out;
ii. sampling/ BEM-FEM simulation—analyze using the BEM–FEM coupled method and obtain blade stress at sampling points;
iii. metamodel construction/fatigue investigation—using the metamodel, investigate fatigue of the composite blade at any given random variables;
iv. parameter sensitivity/effect of water velocity model—study the sensitivities of random variables and effect of water velocity models on the fatigue performance of the blade.

The stall-regulated, horizontal axis, hydrokinetic turbine system consists of three composite blades. Fatigue study was conducted on a blade-to-blade basis. The hydrokinetic loadings, however, were evaluated from a turbine point of view. The stall-regulated turbine system always operates under a fixed rotational speed (60 rpm). The probabilities of failure with respect to different design fatigue lives were analyzed using FORM. Fig. 21 displays the obtained probability of fatigue failure with respect to expected fatigue life ranges (lognormal distribution). The probability of the fatigue life of the turbine blade being less than the designed life (i.e. 20 years) is 5.0684×10^{-4}.

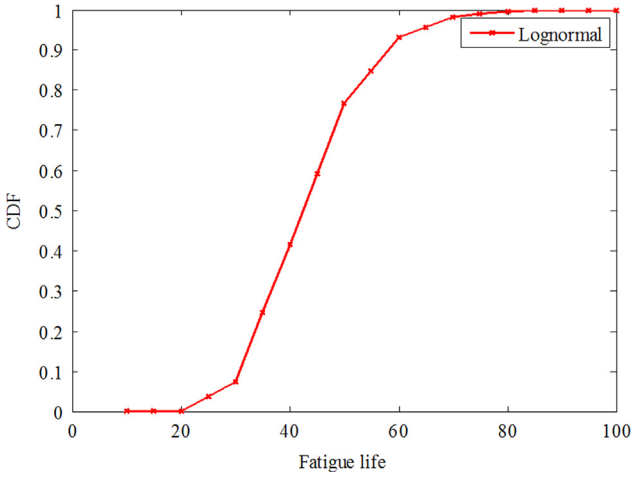

Fig. 21. Probability of fatigue failure with intended fatigue life.

Sensitivity factors (Hu et al., 2012) were used to quantify the relative importance of random variables to the probability of fatigue failure. The sensitivity factor was computed using the MPP:

$$\alpha_i = -u_i^*/\beta \tag{24}$$

where $\alpha_i$is the sensitivity factor of random variable i.

Results indicate that the two parameters of the S–N curve have the highest sensitivity factors, which are -0.6961 and -0.7362, respectively. The result implies that the uncertainties in the S–N curve will affect the fatigue life design significantly. The sensitivity factors of composite material parameters were also compared to analyze the importance of composite material properties. Fig. 22 depicts sensitivity factors for the eight random variables of composite material.

From Fig. 22, both G_{12} and E_{11} contributed negatively to the failure probability; other parameters contributed positively. E_{22}, second ply, and third ply were each more important than other parameters. E_{22} corresponds to the failure mode in terms of the matrix cracking in transverse direction. Second ply and third ply, as the core of the composite lay-up, contribute more than the surface (first ply) and bottom layer (fourth ply).

5.4.1. Effect of water velocity model

The probability of turbine blade failure, for these three distributions, was analyzed to study the effect of river velocity model on the estimation of fatigue life. Fig. 23 plots the fatigue probability of failure with respect to different river velocity distribution models. The fatigue life distribution was found to be only slightly affected by the river velocity model.

6. Conclusion

A methodology for the reliability-based fatigue life investigation of a median scale composite hydrokinetic turbine blade was proposed and studied. The BEM–FEM coupled method was adopted and applied to determine not only the real-time hydrokinetic loadings but also the stress distribution of the composite turbine blade. The model was based on fatigue data from the MSU/DOE fatigue database; constant life diagrams were developed for modified stress ratios and the required fatigue life. A metamodel

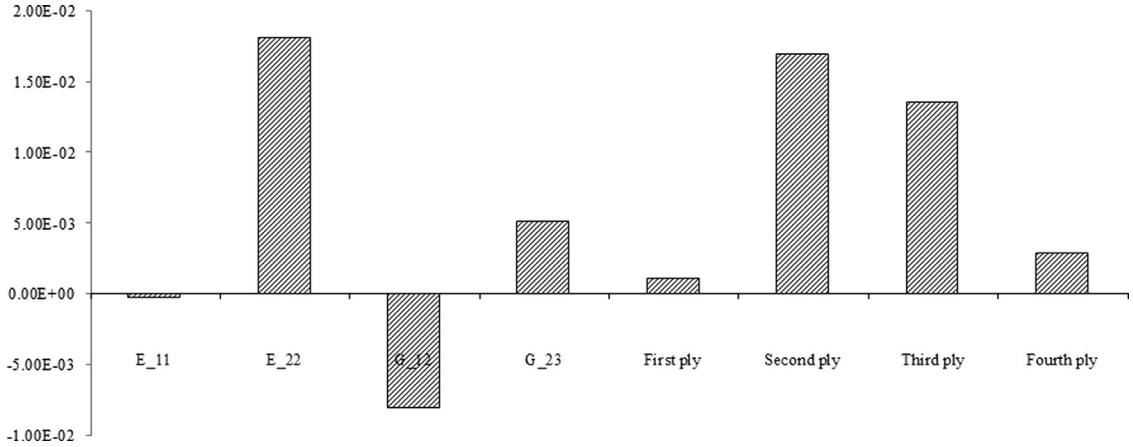

Fig. 22. Sensitivity factors of composite materials.

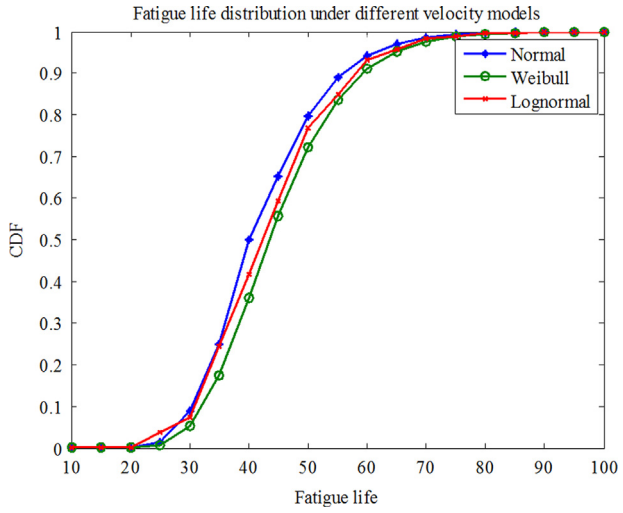

Fig. 23. Fatigue life distribution under different river velocity distribution models.

with respect to stress response was established, addressing the natural variability of material properties/lay-up information. Scatter in *S–N* data on fatigue life distribution and sensitivity of random variables, in terms of stiffness and ply orientation, on probability of fatigue failure were studied. Studies were also performed on the effect of the water velocity model on blade fatigue failure reliability. The composite blade was found capable of operating for more than 20 years. The probability of failure of the composite would increase with time until CDF reached 1. The fatigue failure mode determines the sensitivity of fatigue life to E_{22} (the blade transverse direction). All of the plies contributed positively to the probability of fatigue failure. The second ply and third ply were more important. Although the river velocity model did influence fatigue life distribution, it only slightly influenced the fatigue failure probability. This study suggests the need for a more detailed composite material characterization for hydrokinetic applications. The study provides a complete set of reliability-based fatigue life evaluation methodology for composite blades intended for hydrokinetic applications and can be extended to other fatigue dominant composite structural applications.

Acknowledgment

The authors gratefully acknowledge the support of the Office of Naval Research through Contract ONR N000141010923 (Program Manager – Dr. Michele Anderson).

References

American Society for Testing and Materials (ASTM), 1985. Standard Practices for Cycle Counting in Fatigue Analysis. E1049-85, ASTM Subcommittee E08.04, June 1985 (reapproved 2011).
Anyi, M., Kirke, B., 2010. Evaluation of small axial flow hydrokinetic turbines for remote communities. Energy Sustain. Dev. 14 (2), 110–116 (June).
Buhl, M., 2004. A New Empirical Relationship Between Thrust Coefficient and Induction Factor for the Turbulent Windmill State. NREL/TP-500-36834, September, National Renewable Energy Laboratory, Golden, CO..
Beersma, J.J., Buishand, T.A., 2004. Joint probability of precipitation and discharge deficits in the Netherlands. Water Resour. Res. 40, 1–11.
Berry, D., 2007. Design of 9-meter Carbon-Fiberglass Prototype Blades: CX-100 and TX-100. Sandia National Lab Report 2007-0201, September.
Buckland, H., Masters, I., Chapman, J., Orme, J., Blade element momentum theory in modeling tidal stream turbines, In: Proceedings of the 18th UK Conference on Computational Mechanics, Association of Computational Mechanics in Engineering, Southampton, UK, March 29–31, 2010.
Burges, Christopher J.C., 1998. A tutorial on support vector machines for pattern recognition. Data Min. Knowl. Discov. 2 (2), 121–167.
Chen, W., Tsui, K.-L., Allen, J.K., Mistree, F., 1995. Integration of the response surface methodology with the compromise decision support problem in developing a general robust design procedure, In: Proceedings of the American Society of Mechanical Engineers Technical Conference, pp. 17–20.
Du, X., Chen, W., 2000. Methodology for anaging uncertainty in simulation-based systems design. AIAA J. 38 (8), 1471–1478.
Degrieck, J., Paepegem, W.V., 2001. Fatigue damage modeling of fibre-reinforced composite materials: review. Appl. Mech. Rev. 54 (4), 279–300.
Drela, M., 2006. Xfoil 6.96 for Win32. ⟨http://web.mit.edu/drela/Public/web/xfoil/⟩ (03.05.06.).
Dassault Systèmes, 2010. ABAQUS Version 6.10 User Documentation.
Garrad Hassan & Partner Ltd., 2012. Tidal Bladed Theory Manual (version 4.3). August.
Hashin, Z., 1980. Failure criteria for unidirectional fiber composites. J. Appl. Mech. 47, 329–334.
Hosder, S., Walters, R.W., Balch, M., 2010. Point-collocation nonintrusive polynomial chaos method for stochastic computational fluid dynamics. AIAA J. 48 (12), 2721–2730.
Hu, Z., Li, H., Du, X., Chandrashekhara, K., 2012. Simulation-based time-dependent reliability analysis for composite hydrokinetic turbine blades. Struct. Multidiscip. Optim. 47 (5), 765–781.
Hu, Z., Du, X., 2012. Reliability analysis for hydrokinetic turbine blades. Renew. Energy 48, 251–262.
Jones, D.R., Schonlau, M., Welch, W.J., 1998. Efficient global optimization of expensive black-box functions. J. Global Optim. 13 (4), 455–492.
Khan, M.J., Bhuyan, G., Iqbal, M.T., Quaicoe, J.E., 2009. Hydrokinetic energy conversion systems and assessment of horizontal and vertical axis turbines for river and tidal applications: a technology status review. Appl. Energy 86 (10), 1823–1835 (October).
Kennedy, C.R., Leen, S.B., Bradaigh, M.O., 2011. A study on the fatigue life of glass reinforced polymer composites for tidal turbine blades. In: Proceedings of the Ocean, Offshore and Arctic Engineering Conference, OMAE 2011, ASME, Rotterdam, The Netherlands, June 19–24.
Lange, C.H., 1996. Probabilistic Fatigue Methodology and Wind Turbine Reliability. Sandia National Laboratory Report SAND96-1246.
Li, H., Chandrashekhara, K., Mishra, R.S., 2012. Fatigue life investigation for a medium scale composite hydrokinetic turbine blade. In: Proceedings of the Society for the Advancement of Material and Process Engineering (SAMPE) Conference, Baltimore, Maryland, May 21–24.
Li, H., Chandrashekhara, K., 2012.Structural optimization of laminated composite blade using particle swarm optimization. Proceedings of ASME 2012 International Mechanical Engineering Congress and Exposition (IMECE 2012), Houston, Texas, November 9–15.
Mandell, J.F., Samborsky, D.D., 2010. DOE/MSU composite material fatigue database. Vol. 19, Sandia National Laboratories, SAND97-3002, ⟨http://windpower.sandia.gov⟩ (31.03.10.).
Mahfuz, H., Akram, M.W., 2011. Life prediction of composite turbine blades under random ocean current and velocity shear. In: Proceedings of Oceans 2011, IEEE, Spain, pp. 1–7.
Nijssen, R.P.L., 2006. Fatigue Life Prediction and Strength Degradation of Wind Turbine Rotor Blade Composite (Graduate thesis). November.
Post, N.L., Case, S.W., Lesko, J.J., 2008. Modeling the variable amplitude fatigue of composite materials: a review and evaluation of the state of the art for spectrum loading. Int. J. Fatigue 30 (12), 2064–2086.
Schwartz, S.S. (Ed.), 2006. Proceedings of the Hydrokinetic and Wave Energy Technologies Technical and Environmental Issues Workshop, Washington, DC, October 26–28, 2005, RESOLVE, Inc., ⟨http://hydropower.inl.gov/hydrokinetic_wave/⟩.
Soden, P., Hinton, M., Kaddour, A., 1998. Lamina properties, lay-up configurations and loading conditions for a range of fiber-reinforced composite laminates. Compos. Sci.. Technol. 58, 1011–1022.
Sutherland, H.J., Mandell, J.F., 2005a. Optimized constant-life diagram for the analysis of fiberglass composites used in wind turbine blades. J.. Sol. Energy Eng. 127, 563–569 (November).
Sutherland, H.J., Mandell, J.F., 2005b. The effect of mean stress on damage predictions for spectral loading of fibreglass composite coupons. Wind Energy 8, 93–108.
Shokrieh, M.M., Rafiee, R., 2006. Simulation of fatigue failure in a full composite wind turbine blade. Compos. Struct. 74 (332–242).
Sudret, B., 2008. Analytical derivation of the outcrossing rate in time-variant reliability problems. Struct. Infrastruct. Eng. 4, 353–362.
Samborsky, D.D., Wilson, T.J., Agastra, P., Mandell, J.F., 2008. Delamination at thick ply drops in carbon and glass fiber laminates under fatigue loading. J. Sol. Energy. Eng. 130, 031001-1–031001-8.
Sale, D., Jonkman, J., Musial, W., 2009. Hydrodynamic optimization method and design code for stall-regulated hydrokinetic turbine rotors. In: Proceedings of the 28th ASME International Conference on Ocean, Offshore, and Arctic Engineering, Honolulu, Hawaii, May 31–June 5, NREL/CP-500-45021, American Society of Mechanical Engineers (ASME)..
Viterna, L.A., Janetzke, D.C., 1982. Theoretical and Experimental Power from Large Horizontal-Axis Wind Turbines. NASA TM-82944, National Aeronautics and Space Administration, Washington, DC, September 1982.
Xiu, D., Karniadakis, G.E., 2002. The Wiener–Askey polynomial chaos for stochastic differential equations. SIAM J. Sci. Comput. 24 (2), 619–644.
Young, Y.L., Baker, J.W., Motley, M.R., 2010. Reliability-based design and optimization of adaptive marine structures. Compos. Struct. 92 (2), 244–253 (January).
Zhang, Y.X., Yang, C.H., 2009. Recent developments in finite element analysis for laminated composite plates. Compos. Struct. 88, 147–157.